Progress In Electromagnetics Research, Vol. 135, 317–330, 2013

A 38 TO 44 GHz SUB-HARMONIC BALANCED HBT MIXER WITH INTEGRATED MINIATURE SPIRAL TYPE MARCHAND BALUN

Tom K. Johansen[1, *] and Viktor Krozer[2]

[1]Department of Electrical Engineering, Technical University of Denmark, 348 Oersteds Plads., Kgs. Lyngby 2800, Denmark

[2]Terahertz Photonics, Goethe University, Frankfurt am Main 60438, Germany

Abstract—This work presents an active balanced sub-harmonic mixer (SHM) using InP double heterojunction bipolar transistor technology (DHBT) for Q-band applications. A miniature spiral type Marchand balun with five added capacitances for improved control of amplitude and phase balance is integrated with the SHM. The measured results for the SHM demonstrates a conversion gain of 1.2 dB at an RF frequency of 41 GHz with an associated LO power of 5 dBm. The conversion loss remains better than 3 dB from 38 to 44 GHz. The LO to IF isolation is better than 42 dB within the bandwidth of the mixer and confirms the excellent balance of the integrated spiral type Marchand balun. The DC power consumption of the SHM is only 22.5 mW under normal mixer operation.

1. INTRODUCTION

Sub-harmonic mixers are attractive at millimeter-wave (mm-wave) frequencies as the required local oscillator (LO) frequency can be lowered by a factor of two or more compared to a fundamental frequency mixer [1]. This makes the generation of LO signals with low phase noise less challenging. The most widely used SHM topology at mm-wave frequencies is the anti-parallel diode pair based on high-performance Schottky barrier diodes [2]. Passive resistive FET sub-harmonic mixers also find widespread applications in mm-wave systems [3]. These topologies suffer from high conversion loss and high LO power requirements, but generally exhibit good linearity

Received 2 November 2012, Accepted 19 December 2012, Scheduled 24 December 2012

* Corresponding author: Tom Keinicke Johansen (tkj@elektro.dtu.dk).

performance. It is challenging using similar topologies in HBT based technologies due to the lack of suitable devices. Therefore, it is of great interest to investigate SHM topologies based on active HBT operation at mm-wave frequencies.

Reported SHM topologies based on HBT's can roughly be classified into three categories: 1) Switched Gm-based circuits using stacked LO quads in a Gilbert cell configuration [4]; 2) Balanced transistor pairs followed by IF buffering for selection of the sub-harmonic mixing product [5, 6]; and 3) LO frequency doublers integrated together with a fundamental frequency mixer to enhance the sub-harmonic mixing product of the overall circuit [7, 8]. Recently, the authors demonstrated a novel balanced HBT based SHM topology for E-band wireless applications [9]. The main advantage of the balanced SHM topology is that it eliminates the need for additional IF output buffering and hence reduces power consumption.

In this letter, the theory behind the balanced HBT based SHM topology is derived. A novel design procedure is proposed that is based on even-odd mode analysis to optimize miniature spiral type Marchand balun performance. In order to verify the design procedure a 38 to 44 GHz balanced HBT SHM with integrated miniature spiral type Marchand balun is presented. The experimental results show that the SHM exhibits either positive conversion gain or low conversion loss within its bandwidth together with excellent port to port isolation and low power consumption.

2. BALANCED SUB-HARMONIC MIXER THEORY

A simplified schematic of the balanced sub-harmonic mixer configuration using HBTs is shown in Fig. 1. In order to illustrate the mixing principle it is sufficient to consider a simple exponential transfer current for each HBT of the form $I_c = I_s e^{\frac{V_{be}(t)}{V_t}}$ where I_s is the saturation current, V_t is the thermal voltage, and $V_{be}(t)$ is the base-emitter junction voltage. The LO signal is applied out-of-phase to the base-emitter junctions of the HBTs while the RF signal is applied in-phase. Assuming a voltage signal of the form $V_{be1}(t) = V_b + V_{LO}\cos(\omega_{LO}t) + V_{rf}\cos(\omega_{RF}t)$ across the base-emitter junction of Q_1 the collector current I_{c1} for this HBT can be represented as

$$I_{c1} \approx I_s e^{\frac{V_b}{V_t}} \left(1 + \frac{V_{rf}}{V_t}\cos(\omega_{RF}t)\right) \sum_{n=-\infty}^{n=\infty} \hat{I}_n(x) e^{jn\omega_{LO}t} \qquad (1)$$

where $\hat{I}_n$ represents modified Bessel functions of order n, and $x = V_{LO}/V_t$ is the normalized LO drive level [10]. The above approximation

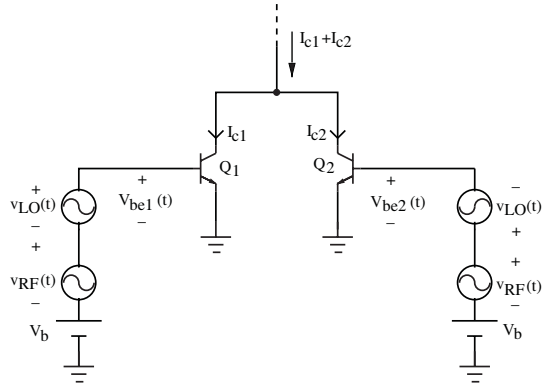

Figure 1. Simplified schematic of balanced sub-harmonic mixer configuration.

assumes that $e^{\frac{V_{rf}}{V_t}\cos(\omega_{RF}t)} \approx 1+\frac{V_{rf}}{V_t}\cos(\omega_{RF}t)$ which is valid for a small-signal RF excitation with $V_{rf} \ll V_t$. Similarly the collector current I_{c2} can be represented as

$$I_{c2} \approx I_s e^{\frac{V_b}{V_t}} \left(1+\frac{V_{rf}}{V_t}\cos(\omega_{RF}t)\right) \sum_{n=-\infty}^{n=\infty} (-1)^n \hat{I}_n(x) e^{jn\omega_{LO}t} \tag{2}$$

if a voltage signal of the form $V_{be2}(t) = V_b - V_{LO}\cos(\omega_{LO}t) + V_{rf}\cos(\omega_{RF}t)$ is assumed across the base-emitter junction of Q_2. Upon summing the two collector currents from Q_1 and Q_2 the following current components occurs

$$\begin{aligned} I_{c1}+I_{c2} \;=\; & 2I_s e^{\frac{V_b}{V_t}} \hat{I}_0(x) \left[1 + \frac{2\hat{I}_2(x)}{\hat{I}_0(x)}\cos(2\omega_{LO}t)\right. \\ & \left. + \frac{V_{rf}}{V_t}\cos(\omega_{RF}t) + \frac{\hat{I}_2(x)}{\hat{I}_0(x)}\frac{V_{rf}}{V_t}\cos((2\omega_{LO}\pm\omega_{RF})t)+\ldots\right] \end{aligned} \tag{3}$$

where the forth term within the square brackets represent the sum and difference sub-harmonic mixing products between the second harmonic of the LO and the RF. The balanced configuration is thus seen to suppress the unwanted fundamental mixing product but enhance the wanted sub-harmonic mixing product. The fundamental LO leakage is also suppressed due to the balanced configuration. The remaining mixing products are easily filtered out. The mixing transconductance g_{mix} can be expressed as

$$g_{mix} = \frac{I_{if}}{V_{rf}} = \frac{2I_s}{V_t} e^{\frac{V_b}{V_t}} \hat{I}_2(x) \tag{4}$$

and is seen to depend on the second order modified Bessel function $\hat{I}_2(x)$. For a given maximum current rating the mixing transconductance is maximized at a conductance angle around 180° which corresponds to a normalized drive level around $x = 4.6$ [10].

3. CIRCUIT DESIGN AND IMPLEMENTATION

The developed theory for the balanced HBT based SHM topology shows that the LO signal should be fed 180 degree out of phase at the bases of Q_1 and Q_2 while the RF signal should be fed in phase. Fig. 2 shows the schematic of our proposed SHM topology which exploits this principle. The SHM design integrates a miniature spiral type Marchand balun at the LO port, an in-phase coupling network at the RF port, and a lumped element IF matching network along with the balanced HBT pair. The in-phase coupling network consists of the inductance L_e, capacitor C_e, and the single-stub matching network of TL_1 and TL_2. The values of the capacitor C_e and inductance L_e should be carefully optimized for highest conversion gain. At a given design frequency there exist an optimum value for the inductance L_e. Too high a value significantly de-generates the mixing transconductance and hence reduces conversion gain while too low a value reduces the coupling of the RF signal into the mixing devices and also reduces conversion gain. The lumped element IF matching network, with the shunt capacitor C_{IF} and series inductor L_{IF}, is chosen as it allows easy injection of the bias supply voltage for the SHM [7].

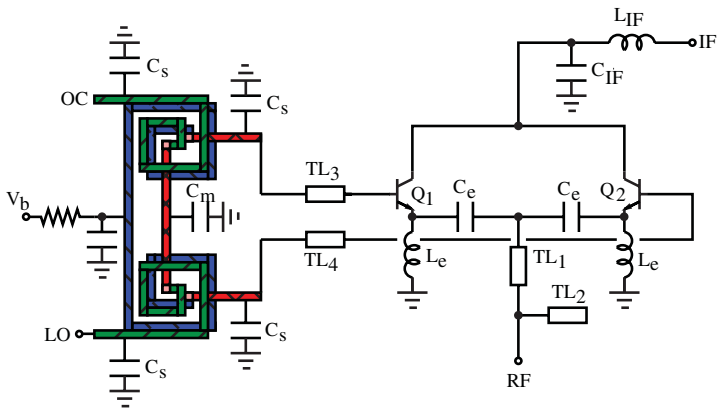

Figure 2. Schematic of SHM with integrated miniature spiral type Marchand balun.

3.1. Balun Optimization

The spiral type Marchand balun is chosen due to its broadband performance compared with alternative integrated balun structures using, e.g., active devices and L-C lumped element hybrids. The balun consists of two offset broadside coupled spiral transformers. Contrary to most other reported miniature spiral type Marchand balun designs, e.g., [11–17], our design adds five shunt capacitors externally to the spiral transformer structures. The lumped element equivalent circuit model of the spiral type Marchand balun configured as a symmetrical four port network is shown in Fig. 3. In this equivalent circuit model C_c and k represents the capacitive and mutual inductive coupling, respectively, for each broadside coupled spiral transformer. The capacitors C_s and C_m represent the externally added capacitors. In [18] the authors presented the design formulas for exact equivalence at the design frequency between the lumped element representation and the standard distributed Marchand balun. Due to limitation in the practical implementation, however, it is often difficult to obtain an exact match with respect to the required capacitive and mutual inductive coupling. As a result, the amplitude and phase balance for the miniature spiral type Marchand balun may deteriorate and the performance of the SHM will suffer. Instead, a design procedure based on an even-odd mode analysis of the symmetrical four port network representation shown in Fig. 3 is proposed. The decomposition of the symmetrical four port network into even- and odd-mode equivalent circuits is shown in Fig. 4. For optimal balun performance the requirements in terms of the even- and odd-mode circuits are [19]

$$T_{even} = 0 \tag{5}$$

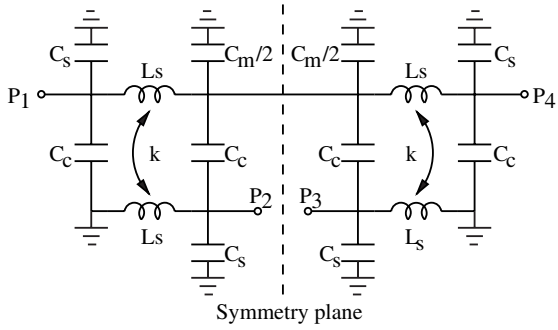

Figure 3. Lumped element symmetrical four port equivalent circuit model of the spiral type Marchand balun.

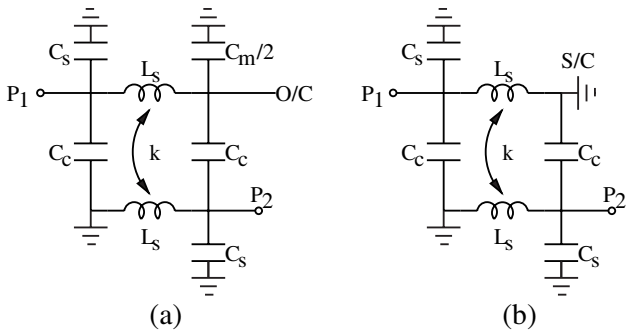

Figure 4. (a) Even-mode and (b) odd-mode circuit for the symmetrical four-port network in Fig. 3.

and

$$\frac{1}{Y_{even}} + \frac{1}{Y_{odd}} = \frac{2}{Y_0} \tag{6}$$

where T_{even} is the transmission coefficient in the even-mode circuit, and Y_{even} and Y_{odd} are the input admittances in the even-mode and odd-mode circuits, respectively, when loaded with $Z_L = 1/Y_L$. The requirement given in (5) of zero transmission in the even-mode equivalent circuit is sufficient to obtain ideal amplitude and phase balance of the balun. To match the input port to the driving impedance $Z_0 = 1/Y_0$ it is also necessary to fulfill (6). The transmission coefficient for the even-mode circuit representation of the spiral type Marchand balun shown in Fig. 4(a) can be expressed as

$$T_{even} = \frac{-2Y_{21e}\sqrt{Y_0 Y_L}}{(Y_0 + Y_{11e})(Y_L + Y_{22e}) - Y_{12e}Y_{21e}} \tag{7}$$

where

$$Y_{11e} = s(C_s + C_c) + \frac{s(C_m/2 + C_c)}{s^2(C_m/2 + C_c)L_s(1-k^2) + 1}, \tag{8}$$

$$Y_{21e} = Y_{12e} = -\frac{(1-k)s(C_m/2 + C_c) - sC_m/2}{s^2(C_m/2 + C_c)L_s(1-k^2) + 1}, \tag{9}$$

$$Y_{22e} = kY_{12e} + \frac{1}{sL_s} + sC_s - \frac{C_c}{C_m/2 + C_c}(Y_{12e} - sC_m/2) \tag{10}$$

represents the admittance parameters of the even-mode equivalent circuit evaluated at the complex frequency $s = j\omega$. To fulfill (5) the relation $C_m = 2(C_c - kC_c)/k$ follows directly from (7) and (9). This is a generalization of the bound given in [18] for exact equivalence with the standard Marchand balun and assures ideal

amplitude and phase balance for the balun even if the capacitive and mutual inductive coupling for the practical spiral transformers deviates from the theoretical values. The four additional shunt capacitors C_s are added to the spiral type Marchand balun to fulfill (6) and thereby provide a good impedance match at the input port. With the provided insight into the design of the miniature spiral type Marchand balun each spiral transformer can be optimized separately using electromagnetic simulation (Momentum) in Agilent ADS.

Figure 5 illustrates the configuration investigated during the EM simulation based optimization procedure. The broadside coupled spiral transformer is implemented on a 120 µm thick InP substrate using three 16 µm wide metal layers (M_1–M_3) separated by polyimide dielectrics. The structure is simulated as a 4-port device with the port designation following that of a standard coupled line. For each simulated offset distance, ΔD, the capacitive and mutual inductive coupling can be extracted from the relations

$$C_c = \frac{\Im\left(Y_{11o} + Y_{12o}\right) - \Im\left(Y_{11e} + Y_{12e}\right)}{2\omega} \tag{11}$$

and

$$k = \frac{\Im\left(\frac{-1}{Y_{12e}}\right) - \Im\left(\frac{-1}{Y_{12o}}\right)}{\Im\left(\frac{-1}{Y_{12e}}\right) + \Im\left(\frac{-1}{Y_{12o}}\right)} \tag{12}$$

where Y_{ije} and Y_{ijo} with $i, j \subset 1, 2$ represent two-port Y-parameters found by driving the spiral transformer in even- and odd-modes, respectively.

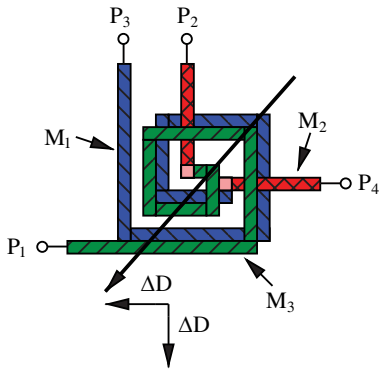

Figure 5. Illustration of offset broadband coupled spiral transformer configuration for EM simulation based optimization. The offset distance is represented by ΔD and the port designation follows that of a standard coupled line.

Table 1 gives the values for the capacitive and mutual inductive coupling at different offset distances extracted from EM simulation at 22.75 GHz along with the target value for the lumped element Marchand balun as calculated from [18]. The resulting optimal value for C_m at each offset distance is also stated. While it is possible to offset the two broadside coupled spirals to reach the target value for either the capacitive or mutual inductive coupling it is not possible to reach both simultaneously. As the design theory shows it is still possible to obtain an optimal balun performance in terms of amplitude and phase balance by imposing the relation $C_m = 2(C_c - kC_c)/k$ to the design.

A miniature spiral type Marchand balun has been implemented as a stand-alone test-structure to verify the design procedure. Fig. 6 shows the experimental results and compares it to the EM simulation of the balun structure. The measurements demonstrates an 1.4 dB loss

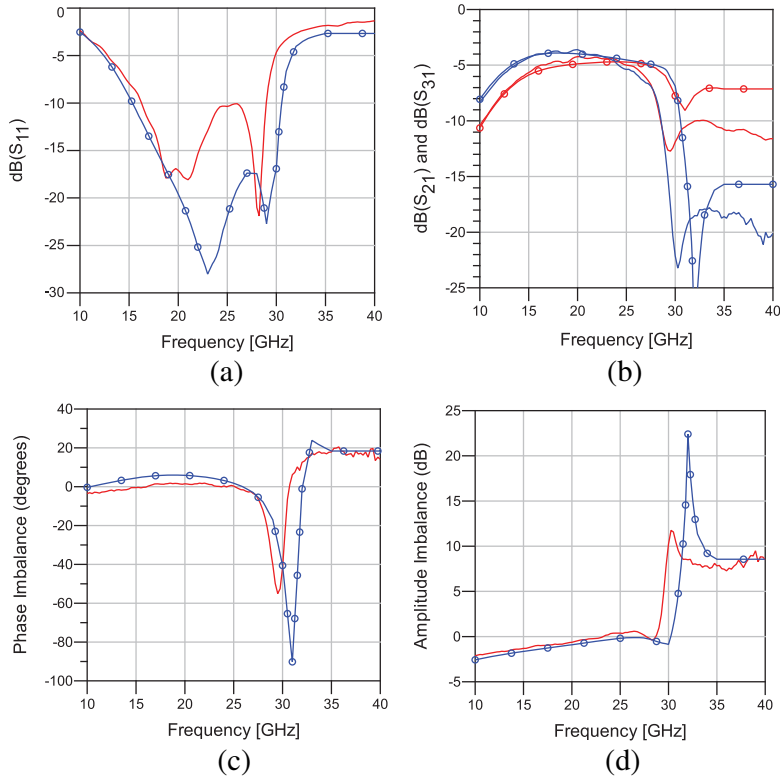

Figure 6. Measured (solid lines) and simulated (solid lines with symbols) balun performance versus frequency. (a) Return loss, (b) insertion loss, (c) phase imbalance, and (d) amplitude imbalance.

Table 1. Capacitive and mutual inductive coupling at different offset distances extracted from EM simulations at 22.75 GHz.

	Target	$\Delta D = 0$ [µm]	$\Delta D = 8$ [µm]	$\Delta D = 16$ [µm]
C_c [fF]	98.8	124.1	106.4	79.4
k	0.577	0.721	0.670	0.576
C_m^* [fF]	144.9	96.0	104.8	116.9

(*Calculated from the relation $C_m = 2(C_c - kC_c)/k$.)

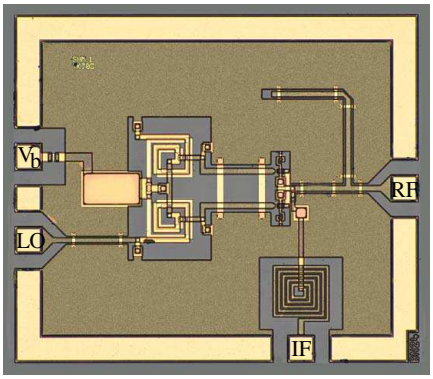

Figure 7. Microphotograph of fabricated SHM with miniature spiral type Marchand balun.

and 13.5 dB return loss at 22.75 GHz. The balun is broadband with a measured 3-dB bandwidth of 15 GHz. An excellent amplitude and phase imbalance of 0.16 dB and 1.0°, respectively, are achieved at the design frequency demonstrating the benefits of the proposed design technique.

3.2. Circuit Implementation

The SHM with optimized spiral type Marchand balun has been implemented in a 1.5 µm InP DHBT circuit oriented technology featuring devices with peak f_T and $f_{\max}$ around 180 GHz and 200 GHz, respectively. The microphotograph is shown in Fig. 7. The chip size is $1.25 \times 1.4\,\text{mm}^2$ including pads. The transmission lines are implemented as coplanar-waveguide (CPW) structures except for TL_3 and TL_4 which are implemented as high impedance asymmetrical coupled transmission lines. The high impedance asymmetrical coupled transmission lines adapts the complex impedance looking into the

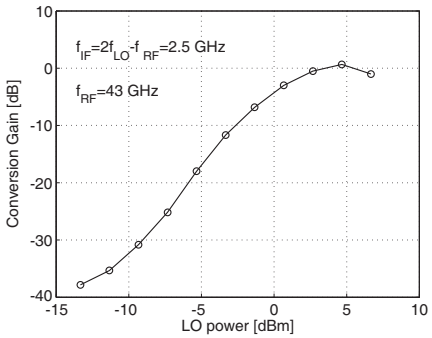

Figure 8. Measured conversion gain versus LO power.

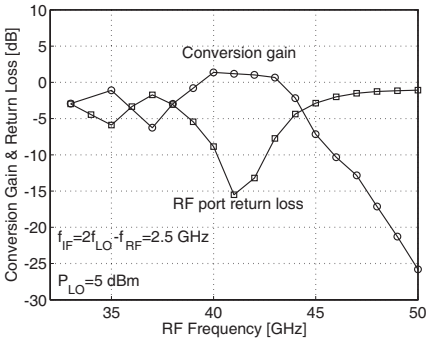

Figure 9. Measured conversion gain and RF port return loss versus RF frequency.

mixing devices to a real load impedance as required by the Marchand balun. With careful optimization of the high impedance asymmetrical coupled transmission lines an impedance level in the 40–50 Ω range results depending on the applied bias voltage and LO signal drive level.

4. EXPERIMENTAL RESULTS

The performance of the SHM is measured via on-wafer probing. An external bias-tee is used to inject the DC biasing for the collectors. Fig. 8 shows the measured conversion gain as a function of LO power at a RF frequency of 43 GHz. The conversion gain reaches a maximum of 0.7 dB at an LO power level around 5 dBm. At this LO power level the circuit draws a current of only 12.5 mA from a 1.8 V supply.

The conversion gain and RF port return loss versus RF frequency for a fixed IF frequency of 2.5 GHz is shown in Fig. 9. At the RF frequency of 41 GHz the RF port return loss is less than −15 dB and the associated conversion gain is 1.2 dB. The conversion loss remains better than 3 dB from 38 to 44 GHz.

The LO-to-IF and RF-to-IF port isolations as a function of RF frequency are shown in Fig. 10. The LO-to-IF and RF-to-IF isolations are better than 42 dB and 20 dB, respectively, for RF frequencies ranging from 33 to 50 GHz. The high level of isolation between the LO and IF port compared with the RF to IF port isolation indicates that an excellent broadband performance has been achieved for the Marchand balun even when integrated with the mixer core.

The IF power versus RF power at an RF frequency of 43 GHz is shown in Fig. 11. The input referred 1 dB compression point $IP_{1\,\mathrm{dB}}$ is

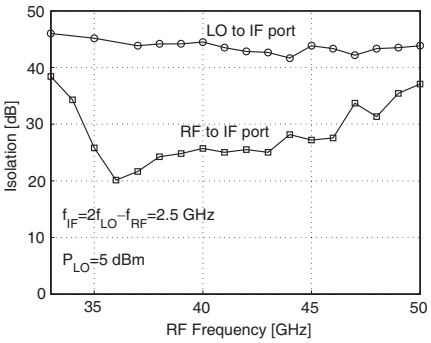

Figure 10. Measured LO-to-IF and RF-to-IF port isolation versus RF frequency.

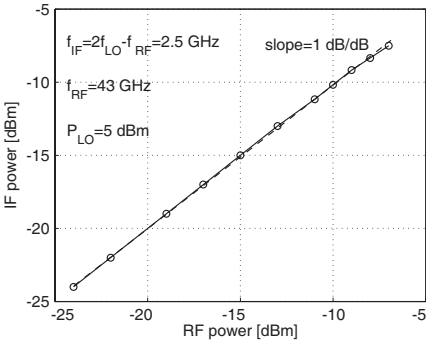

Figure 11. Measured IF power versus RF power. The dashed line follows a slope of 1 dB/dB.

Table 2. Millimeter-wave HBT sub-harmonic mixer performance.

Device Technology (topology)	f_{RF} [GHz]	$C.G.$ [dB]	P_{LO} [dBm]	$IP_{1\,\mathrm{dB}}$ [dBm]	P_{dc} [mW]	Ref.
InP DHBT (balanced w.o IF buffer)	41	1.2	5.0	> -7.0	22.5	This Work
SiGe HBT (balanced w. IF buffer)	77	-10.3^*	10.0	-8.0	62	[5]
SiGe HBT (balanced w. IF buffer)	55	-6.0^*	0.0	-12.5	NA	[6]
InP DHBT (LO doubler+RF preamp)	45	10.3	0.3	-13.0	158	[7]
InP DHBT (LO doubler+RF preamp)	83	1.0	6.0	-9.0	NA	[8]
InP DHBT (balanced w.o IF buffer)	73.5	-4.5	5.0	0	46	[9]
SiGe HBT (anti-parallel diode pair w. IF buffer)	122	-8.0^*	5.0	-5	NA	[20]
SiGe HBT (switched-Gm w. IF buffer)	122	4.0^*	3.0	NA	150	[21]

(*Conversion gain w.o. IF buffer.)

larger than −7 dBm which is the limit of the RF source used during measurements.

Table 2 summarizes the performance of state-of-the-art results for millimeter-wave SHM implemented in HBT technologies. For a fair comparison the conversion gain without IF output buffers are stated. Compared with other published SHM's this work demonstrates an overall good performance with respect to conversion gain, LO power requirements, and linearity. This performance is achieved at the lowest reported power consumption. Despite the focus on HBT technology, the topology can easily be adapted to FET based semiconductor technologies.

5. CONCLUSION

In this paper a 38 to 44 GHz balanced SHM with miniature Marchand balun using InP DHBT technology is presented. The theory behind the balanced HBT based SHM principle is described. A novel practical design approach for miniature spiral type Marchand baluns has been proposed. The design approach is verified by the excellent LO to IF isolation measured on the fabricated SHM with miniature spiral type Marchand balun. Furthermore, the fabricated SHM demonstrates the potential of the balanced SHM topology for providing conversion gain or at least reduced conversion loss at mm-wave frequencies with very low power consumption.

ACKNOWLEDGMENT

The authors would like to thank the III-V Lab, Marcoussis, France, for chip fabrication.

REFERENCES

1. Maas, S. A., *Microwave Mixers*, 2nd edition, Artech House, 1993.
2. Raman, S., F. Rucky, and G. M. Rebeiz, "A high-performance W-band uniplanar subharmonic mixer," *IEEE Trans. Microwave Theory Tech.*, Vol. 45, No. 6, 955–962, Jun. 1997.
3. Lin, S.-K., J.-L. Kuo, and H. Wang, "A 60 GHz sub-harmonic resistive FET mixer using 0.13 µm CMOS technology," *IEEE Microwave and Wireless Components Letters*, Vol. 21, No. 10, 562–564, Oct. 2011.
4. Wu, T.-H., S.-C. Tseng, C.-C. Meng, and G.-W. Huang, "GaInP/GaAs HBT sub-harmonic Gilbert mixers using stacked-

LO and leveled-LO topologies," *IEEE Trans. Microwave Theory Tech.*, Vol. 55, No. 5, 880–889, May 2007.

5. Hung, J., T. M. Hancock, and G. M. Rebeiz, "A 77 GHz SiGe sub-harmonic balanced mixer," *IEEE J. Solid-State Circuits*, Vol. 40, No. 11, 2167–2173, Nov. 2005.
6. Perumana, B. G., S. Chakraborty, S. Sarkar, P. Sen, D. A. Yeh, A. Raghavan, D. Dawn, C. Lee, S. Pinel, and J. Laskar, "A SiGe sub-harmonic mixer for millimeter-wave applications," *Proc. 2nd EuMIC Conf.*, 80–83, Munich, Germany, Oct. 2007.
7. Johansen, T. K., J. Vidkjær, V. Krozer, A. Konczykowska, M. Riet, F. Jorge, and T. Djurhuus, "A high conversion-gain Q-band InP DHBT subharmonic mixer using LO frequency doubler," *IEEE Trans. Microwave Theory Tech.*, Vol. 56, No. 3, 613–619, Mar. 2008.
8. Ning, X., H. Yao, Y. Su, X. Wang, J. Ge, Z. Jin, and X. Liu, "A 79 GHz sub-harmonic mixer design using a 1 μm InP DHBT technology," *Proc. ICMMT*, 446–449, 2012.
9. Johansen, T. K. and V. Krozer, "An InP HBT sub-harmonic mixer for E-band wireless communication," *Proc. 5th EuMIC Conf.*, 198–201, Paris, France, Sep. 2010.
10. Johansen, T. K., V. Krozer, J. Vidkjær, and T. Djurhuus, "A novel HBT frequency doubler design for millimeter-wave applications," *Proc. INMMIC*, 106–109, Jan. 2006.
11. Yoon, Y. J., Y. Lu, R. C. Frye, M. Y. Lau, P. R. Smith, and D. P. Kossives, "Design and characterization of multilayer spiral transmission-line baluns," *IEEE Trans. Microwave Theory Tech.*, Vol. 47, No. 9, 1841–1847, 1999.
12. Lee, Y.-C., Y.-H. Chang, S.-H. Hung, W.-C. Chien, C.-C. Su, C.-C. Hung, C.-M. Lin, and Y.-H. Wang, "A single-balanced quadruple subharmonic mixer with a compact IF extraction," *Progress In Electromagnetics Research Letters*, Vol. 24, 159–167, 2011.
13. Lee, Y.-C., C.-M. Lin, S.-H. Hung, C.-C. Su, and Y.-H. Wang, "A broadband doubly balanced monolithic ring mixer with a compact intermediate frequency (IF) extraction," *Progress In Electromagnetics Research Letters*, Vol. 20, 175–184, 2011.
14. Su, J.-Y., C. Meng, P.-Y. Wu, and G.-W. Huang, "0.13-μm CMOS Q-band leveled-LO subharmonic mixer with injection-locked frequency divider quadrature generator," *Microwave Opt. Technol. Lett.*, Vol. 51, No. 11, 2663–2665, 2009.
15. Fu, J. S., C.-Y. Kuo, S.-W. Lin, P.-Y. Ke, and H.-C. Chiu, "A

wideband Gilbert cell mixer with an integrated Marchand balun using 0.5-μm GaAs enhancement-mode pHEMT technology," *Microwave Opt. Technol. Lett.*, Vol. 52, No. 6, 1302–1306, 2010.

16. Huang, C.-H., C.-H. Chen, Y.-C. Lin, and T.-S. Horng, "Design and analysis of spiral-type Marchand balun using physical transformer model on glass integrated passive device substrate," *Microwave Opt. Technol. Lett.*, Vol. 53, No. 9, 2011–2016, 2011.
17. Huang, C.-H., T.-S. Horng, C.-C. Wang, C.-T. Chiu, and C.-P. Hung, "Optimum design of transformer-type Marchand balun using scalable integrated passive device technology," *IEEE Trans. Comp. Packag. Technol.*, Vol. 2, No. 8, 1370–1377, 2012.
18. Johansen, T. K. and V. Krozer, "Analysis and design of lumped element Marchand baluns," *Proc. MIKON*, 53–56, Wroclaw, Poland, May 2008.
19. Ang, K. S., Y. C. Leong, and C. H. Lee, "Analysis and design of miniaturized lumped-distributed impedance-transforming baluns," *IEEE Trans. Microwave Theory Tech.*, Vol. 51, No. 3, 1009–1017, Mar. 2003.
20. Sun, Y. and C. J. Scheytt, "A 122 GHz sub-harmonic mixer with a modified APDP topology for IC integration," *IEEE Microwave and Wireless Components Letters*, Vol. 21, No. 12, 679–681, Dec. 2011.
21. Müller, A., M. Thiel, H. Irion, and H.-O. Ruoss, "A 122 GHz SiGe active subharmonic mixer," *Proc. 13th GAAS Symp.*, 57–60, Paris, France, Oct. 2005.